

Testing Flight Paths for Collecting 3D LADAR Imagery of Inconspicuous Targets

Mewett, D.T.¹, M.D. Graham¹ and A.H. Davies¹

¹ *Defence Science and Technology Organisation, Edinburgh, South Australia*
Email: david.mewett@dsto.defence.gov.au

Abstract: A pilot study was performed to examine flight paths for an airborne foliage-penetrating Laser Detection and Ranging (LADAR) three-dimensional (3D) imaging system. Such systems form 3D images based on time-of-flight of laser photons, some of which pass through gaps in foliage or other partial obscurers such as camouflage nets. Hence the 3D image will contain partial information about any objects behind or underneath such obscurers. The obscurer can be removed from the image by only keeping points within some appropriate range, leaving a partial image of the hidden objects which may include targets of interest. An improved overall image can be formed by combining images taken from several different viewpoints, using knowledge of the LADAR sensor's location at each viewpoint. In this study, we compared the overall 3D images obtained from an airborne LADAR system during different flight paths.

The scene for each flight path consisted of a four-wheel-drive vehicle placed in a section of a eucalypt forest. Models for the vehicle and the individual trees were created in the 3D modelling software Maya, and exported as point clouds to be used in the general-purpose analysis software MATLAB. The overall forest scene was then assembled from the individual trees. The amount of light penetrating the foliage was determined at three different locations within the scene. On average, results were found to roughly agree with the prediction that light penetration scales with the sine of the angle from horizontal.

Formation of LADAR images was modelled by determining the set of points in the scene that had a direct line-of-sight to the airborne sensor. This low-fidelity approach was taken because the aim of the study was to investigate ways of tasking the sensor system, rather than using the model as part of a hardware design process or a testbed for data processing algorithms. Since there is already a random effect due to line-of-sight through the forest canopy, it was decided that further random effects leading to false returns or missed returns would unnecessarily complicate the comparison between results from different flight paths.

The flight paths in this study were intended to keep the sensor footprint directed at a known or assumed target area on the ground. One type of path was an arc centred at this location, with the sensor constantly directed sideways at an appropriate elevation. The other type of path went straight past the target area, with the sensor needing to be constantly redirected. Different scan spacings along the path were also investigated. It was assumed that the unobscured view from each flight path would be sufficient for the surveillance or reconnaissance task. So for each flight path, the Hausdorff distance was calculated as a measure of the difference between the 3D image of the target taken through the foliage and the corresponding unobscured image from the same flight path. No significant difference was found between results for the straight and arc paths, but the 3D images were closest to the unobscured views for the smallest scan spacing.

Keywords: *laser radar, sensor tasking, foliage penetration*

1. INTRODUCTION

Laser Detection and Ranging (LADAR) systems measure the time it takes for transmitted laser pulses to return to a detector, thereby measuring the distance to objects from which the pulses were reflected. If a scene of interest is flood-illuminated with a laser and the returned pulses are focused onto an array of detectors, then the spatial location of points in the scene can be determined relative to the sensor and used to produce three-dimensional (3D) images.

Each detector in the array can receive multiple returns, so the image can be restricted to a desired range of depths. Such a system can be used to image objects partially obscured by foliage or camouflage netting. Since the returns from a target may be too sparse to allow recognition in a single 'snapshot', a foliage-penetrating LADAR imaging system combines multiple images taken at differing views through the foliage. These views can be obtained by placing the sensor in one position and relying on wind to move the foliage by causing branches to sway (Schilling *et al.* 2002), or by placing the sensor on a moving platform such as an aircraft (Aull and Marino 2005). In the case of a moving platform, GPS and inertial navigation system information is used to georegister the 3D images before they are combined.

This paper describes a pilot study conducted to compare flight paths for a hypothetical airborne LADAR imaging system, searching for targets in an Australian open woodland environment. It is envisioned that should the Australian Army consider procuring such a system in the future, studies following from this will be required to determine how to operate the system most effectively.

The overall approach in the study was to:

1. Create 3D models of trees and targets, and assemble into a forest scene.
2. Form 3D images of the target from LADAR scans at intervals along appropriate flight paths, both with and without the trees present ('obscured' and 'unobscured' views, respectively).
3. Compare the differences between the obscured and unobscured results.

2. TREE AND TARGET MODELLING

2.1. 3D modelling

Models of trees and a target vehicle were developed using the software packages Maya¹ and MATLAB².

Tree models were created in the 3D modelling software package Maya (Figure 1), with dimensions based on a survey conducted near RAAF Tindal, Northern Territory (Williams *et al.* 2003). The overall appearance was based on photos of poplar box (*Eucalyptus populnea*) from the Injune Landscape Study Site in central Queensland (A. Lee, pers. comm.). A 4-wheel drive vehicle model (Figure 1c) was obtained from a 3D model website (<http://jahansibi.page.tl/>, accessed 4 February 2008).

To export the Maya models to MATLAB for further manipulation, a procedure was developed which made use of Z-buffer images. The Z-buffer is the component of Maya's native output format which indicates furthest visible depth. The Z-buffer was extracted and manipulated to export to MATLAB via a plug-in module developed using C++ libraries that are part of the Maya package. A series of four Z-buffer images (e.g. Figure 1) were captured at 90° intervals around each tree and target model, using an orthographic projection so as not to introduce perspective distortion. A fifth Z-buffer image was also taken from above each model to provide a top-down view. These image files were then passed to MATLAB, where the image pixel coordinate pairs and the Z-buffer depth values were used to produce a list of voxels (volume elements) in 3D space. This list forms a point cloud representation of the model. The list could also potentially contain the surface reflectivity of each voxel, but we chose not to include reflectivity because the type of sensor assumed in §3.1 is not sensitive to the intensity of the returned pulse.

Scenes were constructed from the individual tree and target models by first shifting their *x* and *y* coordinates, then including the shifted models in an overall list of voxels describing the scene. The scene in this study had characteristics of an 'open forest', i.e. 10–30 m high trees with 30–70 % foliage cover (Specht 1970), and consisted of 49 trees within a circular area of approximately 50 m diameter. There were 18 trees between 20–30 m high, 23 trees between 10–20 m high, and 8 trees less than 5 m high. A flat target was used for light penetration tests, as described in the next section. For the rest of the study, the target vehicle was located towards the centre of the scene in a position that a vehicle could have conceivably driven to in between the tree trunks.

¹ Autodesk, Inc., San Rafael CA, USA

² The MathWorks, Inc., Natick MA, USA

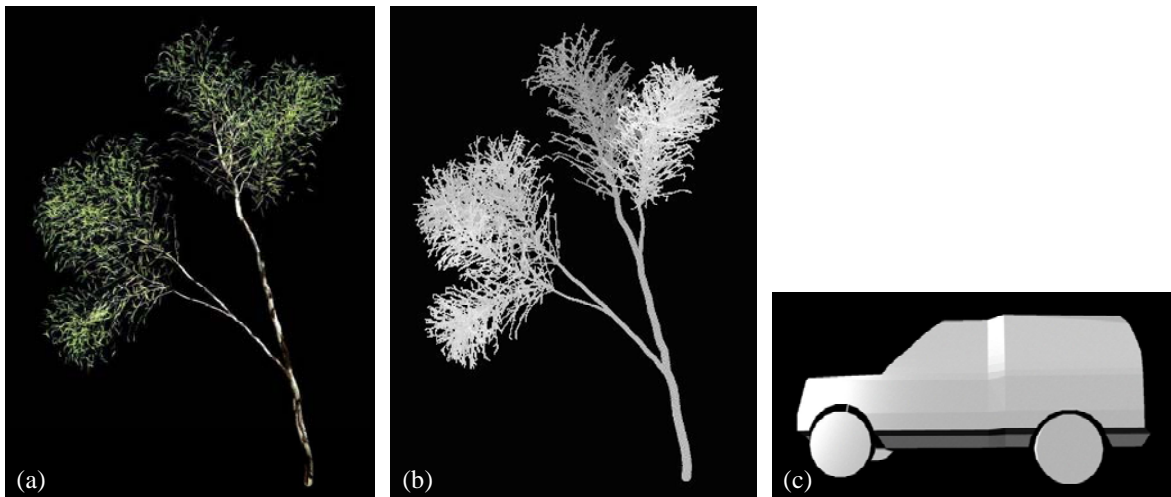


Figure 1. Models produced using Maya. (a) Rendered image of a tree model. (b) Z-buffer image of the tree. (c) Rendered image of target vehicle (not shown to scale with the tree model).

2.2. Light penetration of the forest model

The forest model was verified by determining the light penetration through the canopy as a function of depression angle. If the forest canopy can be considered to be roughly homogenous, then the light penetration is expected to be $T_{vert} \sin \theta$ where θ is the depression angle, i.e. angle from horizontal (Chevalier *et al.* 2007).

Foliage penetration was estimated by ray tracing through the forest for depression angles between 45°–90° at 15° azimuth increments for each of three locations in the forest scene. The software developed to form the LADAR 3D images (see §3.2) was used for this calculation, by determining the number of rays to reach a flat target on the ground. Sensor and aircraft parameters were set so that the maximum sensor footprint width was 10 m and the slant range of the centre ray was 700 m for all sensor depression angles. For locations towards edges of the scene, only 180° of azimuth was used so that all rays entered the canopy from above and not from the sides of the trees.

A least-squares fit to the results gave $T_{vert} = 31.3\%$ (Figure 2), although a straight line was found to give a better fit than the sine function. Since the canopy was of course not a homogenous medium, there was considerable variation in the light penetration at each depression angle.

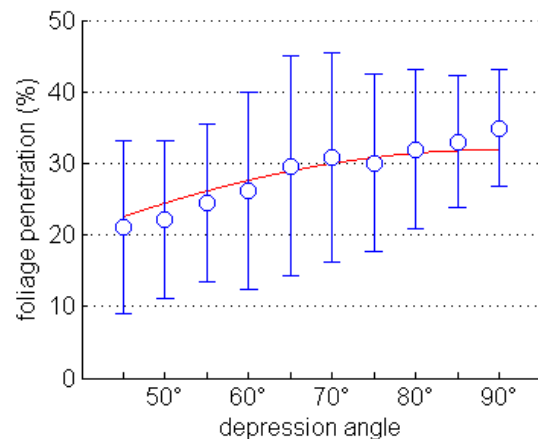


Figure 2. Measured light penetration of the forest canopy model (○ mean ± 1 standard deviation) and predicted penetration (solid red line).

The light penetration results have implications for designing flight paths. The greatest penetration of the canopy is achieved when the sensor is pointed straight down. But only the top surfaces of the target would be imaged in this case, and we expect that returns from the sides of targets would also be required to allow identification of many targets. For this forest, the flight path should give some snapshots at depression angles between 70°–90° where the expected penetration is approximately 30%.

3. LADAR SYSTEM MODELLING

The hypothetical LADAR system in this study is assumed to consist of a Geiger-mode avalanche photodiode (APD) array LADAR sensor such as those developed at MIT Lincoln Laboratory (Aull *et al.* 2002), mounted in a stabilised, gimballed turret on a tactical uninhabited aerial vehicle (TUAV). Geiger-mode APD detectors are essentially photon counters and, unlike linear-mode APD detectors, do not distinguish between the amplitudes of returned pulses.

3.1. Sensor

While high fidelity models of LADAR sensors have been developed to aid in the design process and for testing data processing techniques (O'Brien & Fouche 2005, Budge *et al.* 2006), a lower fidelity model was used here since this study was aimed at how to use the assets most effectively rather than creating a detailed model for simulating the sensor itself.

The sensor was characterised by:

- the number of detectors in the array (128×128 pixels);
- the pitch between detectors ($100 \mu\text{m}$);
- the field of view (1.5°);
- depth resolution, i.e. the spacing between returns from a single detector (3 m);
- the number of rays that are received by each detector in the array (16 rays).

A single large array was assumed (Stettner *et al.* 2005) rather than the approach of a smaller array with scanning optics as used in the MIT Lincoln Laboratory system. Depth resolution refers to the minimum spacing between subsequent returns from the same detector, and should not be confused with the accuracy of a given range measurement. For Geiger-mode APD detectors, the time between subsequent detections is determined by the time taken to reset a detector, which is 10 ns for the MIT Lincoln Laboratory sensors. The number of rays per detector models the reception of multiple photons from within the field of view of an individual detector. The depth resolution parameter was used to determine which of these returns to keep.

Each detector in the model only receives correct detections. In real sensors, quantum effects lead to probabilities of true and false detections of photons, jitter in the timing of output pulses, and crosstalk between adjacent detectors. The resolution of the timing circuit can also introduce errors, and some clutter returns may be received from airborne particles. However, these effects were ignored and an ideal error-free sensor model was used instead so that the only random effect was the difference in foliage penetration from different look directions.

3.2. Ray Tracing

The reflection of the laser pulse from the scene back to the sensor was modelled by determining which voxels had a direct line-of-sight to the sensor. Physical effects such as the reflectivity of different surfaces were omitted, since reflectivity (and hence the amplitudes of returned pulses) is less important for Geiger-mode APD sensors than for linear-mode sensors. Rays are traced from the sensor grid and through the 3D model of the scene under the assumption that the rays are equally spaced in angle and do not cross. The rays are defined by the overall pointing direction of the sensor, the field of view and the number of rays. To make it easier to compare results from different flight paths, it was decided to leave the results of this modelling as being the set of voxels that contribute to the 3D image (Figure 3), rather than constructing the correct angle-angle-range image that such a sensor would actually produce.

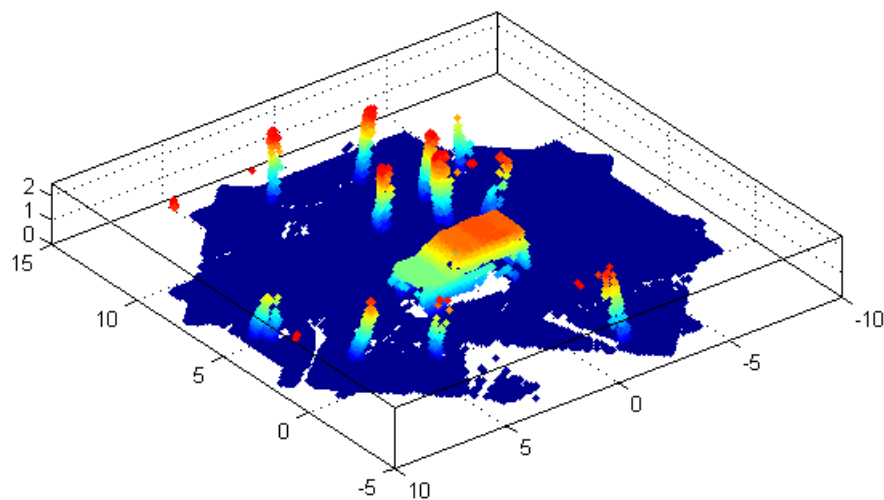


Figure 3. Example simulation output after a threshold has been applied to remove the tree canopy and reveal the vehicle from Figure 1c. All values are given in metres. Colour corresponds to height (z axis).

3.3. Sensor Platform

Rather than explicitly modelling the flight of an aircraft carrying a LADAR sensor, the flight path is simply represented as a sequence of scan locations. Four parameters are defined at each scan location: aircraft position; aircraft heading; sensor azimuth angle relative to the aircraft; and sensor depression angle relative to horizontal (i.e. including the aircraft’s angle of bank).

4. CONDUCTING THE PILOT STUDY

4.1. Design of Flight Paths

Let us assume that the concept of operation for a LADAR imaging system is a reconnaissance role where the sensor is cued to image a patch of ground in which a target is believed to be located. (An area search could be conducted by ‘tiling’ many such patches.) As stated earlier, multiple views through the foliage are required to build up a recognisable 3D image of a concealed target. These views can be achieved by varying the sensor azimuth angle to the target, the aircraft’s standoff range to the target, the aircraft’s altitude, or combinations of these. Varying the altitude repeatedly reduces the endurance of aircraft, and so we have not considered such flight paths. The standoff range can be varied by flying a straight and level path over the target while keeping the sensor directed at the target location. The sensor azimuth can be varied by flying in an arc around the target while keeping the sensor at a fixed azimuth and depression. The sensor azimuth and standoff range can be varied together by flying a straight and level path past the target while keeping the sensor directed at the target location. Therefore, the types of path to consider are really only arc paths (Figure 4a) and straight paths (Figure 4b).

Arc flight paths are potentially constrained by the minimum turning radius of the aircraft. By balancing the centripetal force and the horizontal component of the lift force during the turn, the following expression for the radius of the turn r is obtained (Houghton & Carruthers 1982):

$$r = \frac{v_{TAS}^2}{g \tan \theta} = \frac{v_{IAS}^2}{(\rho_A / \rho_0) g \tan \theta}$$

where v_{TAS} is the true airspeed, g is acceleration due to gravity, θ is the angle of bank, v_{IAS} is the indicated airspeed, ρ_A is the air density at the aircraft altitude and ρ_0 is the air density at sea level. The conversion from indicated airspeeds to true airspeeds is appropriate for low speeds (i.e. well below the speed of sound) where compressibility effects are not expected. Air densities are taken from the International Standard Atmosphere (ISO 2533:1975).

For UAVs such as the Shadow 200 that are candidates for consideration by the Australian Defence Force (Muir 2008), speeds encompassing loitering and cruise speeds are in the order of 65–85 knots (*Unmanned Vehicles Handbook* 2006). Choosing an altitude of 5000 ft, an indicated airspeed of 85 knots, and an angle of bank of 60°, then the aircraft would turn about a radius of 130.5 m. This corresponds to a sensor depression angle of 85° if the aircraft were turning around the target location. For an indicated airspeed of 65 knots, the aircraft would turn about an even tighter radius of 76 m, corresponding to a depression angle of 87°. Such steep sensor depression angles would result in few returns from the sides of a target. Therefore, an appropriate radius of turn for arc paths is greater than the minimum. Since the flight of the aircraft was not explicitly modelled, it was not necessary to choose a combination of speed and angle of bank.

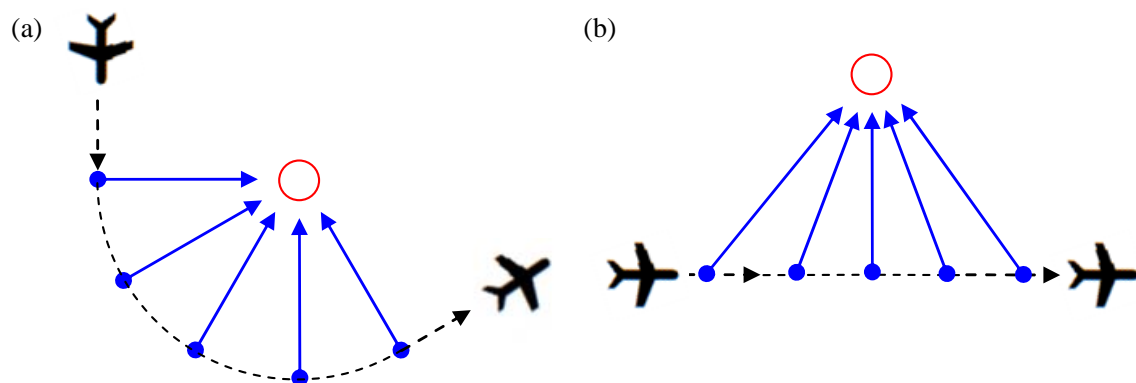


Figure 4. Flight paths. Red indicates the targeted area, blue arrows indicate individual scans.

For the purpose of a pilot study, we decided to compare two factors: the flight path type and the separation between individual scans along the path. Other factors that might be considered in a longer study include the altitude of the flight path, the sensor depression angle, and the length of the flight path. The longest arc flight path would be a complete circle.

The common parameters chosen for the pilot study were:

- 5000 ft altitude;
- 268.7 m arc radius / straight path closest point of approach, giving 80° sensor depression angle;
- 46.9 m minimum scan spacing, corresponding to 10° for the arc paths;
- 562.8 m path length, corresponding to 120° for the arc paths.

Arc paths were created by locating scans at 5° intervals in a circle centred at the target and then grouping scans into overlapping 120° blocks. A straight path was created tangential to the centre scan of each arc path, with 13 scans along the path. A total of 936 individual scans were required. Results were generated using five different scan spacings: 46.9 m, 93.8 m, 140.7 m, 187.6 m and 281.4 m (equivalent to 10°, 20°, 30°, 40° and 60° respectively for the arc paths). This resulted in 72 paths for each combination of path type and spacing.

4.2. Measure of Performance

Two 3D images of the target were reconstructed for each flight path. The first was the ‘obscured’ view of the target through the trees. The second was the ‘unobscured’ view of the target without the trees present, i.e. the ideal view from a given flight path. Assuming that the unobscured view would be sufficient for the surveillance mission, which flight path results in the least expected difference from the unobscured view?

The difference between the obscured and unobscured views for a given flight path was measured by the Hausdorff distance between the 3D images. Let A be the set of points that make up the obscured view and B be the set of points that make up the unobscured view. Then A and B are within Hausdorff distance d of each other if and only if every point of A is within distance d of some point of B , and every point of B is within distance d of some point of A (Edgar 1990). The Euclidean distance was chosen as the basic distance metric.

5. RESULTS

The Hausdorff distance results for the arc flight paths are shown in Figure 5. Results for the straight paths were very similar, and so are not shown.

A two-way analysis of variance (ANOVA) test indicated that the choice of arc or straight path had no significant effect on the Hausdorff distance results ($p > 0.2$) while the choice of scan spacing was significant ($p < 0.0001$), but there was no significant interaction between these effects ($p > 0.9$). A Tukey’s HSD multiple comparison test was used to investigate the effect of scan spacing (Table 1). The mean Hausdorff distance result for the smallest scan spacing was significantly less than the mean result for the other four spacings.

A Lilliefors test indicated that the distribution of residuals in the ANOVA model was significantly different to normal ($p < 0.001$); a normal probability plot showed that this difference was in the tails of the distribution, particularly the upper and lower deciles. Instead of attempting to achieve a closer fit to a normal distribution by transforming the data, we instead performed Friedman’s ‘nonparametric ANOVA’ tests on the Hausdorff distance results. The Friedman’s tests agreed with the ANOVA results, confirming that the choice of arc or straight path had no significant effect ($p > 0.5$) while the choice of scan spacing had a significant effect ($p < 0.0001$).

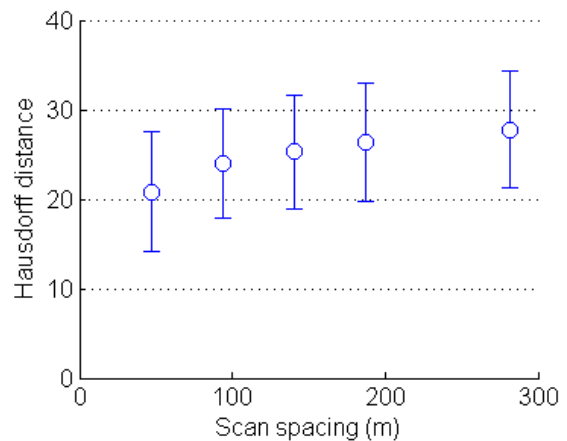


Figure 5. Hausdorff distance results (mean ± 1 standard deviation) for the arc paths.

6. DISCUSSION AND CONCLUSIONS

It was initially expected that the arc paths would give results closer to the ideal, since a constant depression angle is maintained in these paths. But the depression angle only varied from 75°–80° along the straight paths, which is within the range identified from Figure 2. The difference between arc and straight paths might be more significant for a smaller radius of turn or a greater path length.

The results suggest that whether a straight or arc path is chosen, it is preferable to take scans as close together as possible. For the straight path, the sensor must turn in between scans and so the minimal spacing will be limited by the slew rate of the turret housing the sensor. But more scans mean more data, which will ultimately need to be sent to a ground station. The data volume could be reduced by removing returns above the expected height of a target before transmitting the data from the aircraft, but the number of scans contributing to the data may still need to be managed.

It was assumed that a sensor depression angle of 80° or less is required to give sufficient shape information about the sides of the target. Shape information is important for identification, but suitability of the results for identification was not assessed in this study. Instead, it was assumed that the unobscured view would be sufficient in each case. Longer arc paths may prove to provide better data for target identification.

Further work is required to investigate the effects of sensor depression angle and flight path length. Also, it is not known whether the results for the ‘open forest’ modelled in this study will apply to either more or less densely forested areas. Discussions have commenced with CSIRO to consider using sampled data from real forests rather than the modelled forest in future studies.

ACKNOWLEDGMENTS

Brian Rebbeschi and Howard Quick of Air Vehicles Division, DSTO provided advice on aircraft dynamics.

REFERENCES

Aull, B., A. Loomis, D. Young, R. Heinrichs, B. Felton, P. Daniels, and D. Landers, (2002), Geiger-mode avalanche photodiodes for three-dimensional imaging. *Linc. Lab. J.*, 13(2), 335–350.

Aull, B. and R. Marino, (2005), Three-dimensional imaging with arrays of Geiger-mode avalanche photodiodes. *Proc. SPIE*, 6014, article 60140D.

Budge, S., B. Leishman, and R. Pack, (2006), Simulation and modeling of return waveforms from a ladar beam footprint in USU LadarSIM. *Proc. SPIE*, 6214, article 62140N.

Chevalier, T., O. Steinvall, and H. Larsson, (2007), Performance of laser penetration through forest vegetation, *Laser Radar Technology and Applications XII*, Proceedings of SPIE, 6550, article 65500Q.

Edgar, G.A. (1990) *Measure, Topology, and Fractal Geometry*, Springer-Verlag, New York USA, pp. 65–66.

Houghton, E.L. and N.B. Carruthers, (1982), *Aerodynamics for Engineering Students*, 3rd edn, Edward Arnold, London, UK, pp. 49 & 598.

Lee, A. (Australian National University), photographs supplied via email, 17 November 2005.

Muir, T. (2008), What lies ahead for JP129 TUAV? *Aust Defence Mag*, 16(11), 38–40.

O’Brien, M. and D. Fouche, (2005), Simulation of 3D Laser Radar Systems. *Linc. Lab. J.*, 15(1), 37–60.

Schilling, B.W., D.N. Barr, G.C. Templeton, L.J. Mizerka, and C.W. Trussell, (2002), Three-dimensional imaging of obscured targets by multiple-return laser radar. *23rd Army Science Conference*, Orlando, Florida, 2–5 Dec 2002, paper JO-01.

Specht, R.L. (1970), Vegetation, in G.W. Leeper (ed), *Australian Environment* 4th edition, Melbourne University Press, Melbourne.

Stettner, R., H. Bailey, and S. Silverman, (2005), Large format time-of-flight focal plane detector development. *Proc. SPIE*, 5791, 288–292.

Unmanned Vehicles Handbook 2006, December 2005, Shephard Press, UK, p. 30.

Williams, P., C. Stanford, D. Sanderson, K. Pash, and D. Lohmeyer, (2003), *A Vegetation Canopy Probability Line of Sight Model*, DSTO technical report DSTO-TR-1402.

Table 1. Multiple comparison results

Scan spacing pair (m)		Means significantly different?
46.9	93.8	yes
46.9	140.7	yes
46.9	187.6	yes
46.9	281.4	yes
93.8	140.7	no
93.8	187.6	yes
93.8	281.4	yes
140.7	187.6	no
140.7	281.4	yes
187.6	281.4	no